OPTIMIZATION OF THERMOELECTRIC ENERGY HARVESTER TO POWER WIRELESS ONBOARD BEARING HEALTH SENSOR DURING RAIL SERVICE

A Thesis

by

DANNA CECILIA CAPITANACHI AVILA

Submitted in Partial Fulfillment

of the Requirements for the Degree of

MASTER OF SCIENCE IN ENGINEERING

Major Subject: Mechanical Engineering

The University of Texas Rio Grande Valley

July 2025

OPTIMIZATION OF THERMOELECTRIC ENERGY HARVESTER TO POWER WIRELESS ONBOARD BEARING HEALTH SENSOR DURING RAIL SERVICE

A Thesis

by

DANNA CECILIA CAPITANACHI AVILA

COMMITTEE MEMBERS

Dr. Constantine Tarawneh
Chair of Committee

Dr. Heinrich Foltz
Co-chair of Committee

Dr. Arturo Fuentes
Committee Member

July 2025

ABSTRACT

Capitanachi Avila, Danna, C. Optimization of Thermoelectric Energy Harvester to Power Wireless Onboard Bearing Health Sensor During Rail Service. Master of Science in Engineering (MSE), July 2025, 51 pp., 4 tables, 29 figures, 32 references.

This work presents the optimization of a thermoelectric energy harvester designed to supply power to a wireless onboard bearing health monitoring device for critical freight rail components. The study demonstrates an enhancement in the circuitry through the integration of an energy management subsystem (E-Peas AEM20940), which features a boost converter with lower self-start voltage. The harvesting system was tested on dynamic bearing test rigs to closely replicate field service conditions. Test plans were conducted using common freight speeds and loads to simulate a representative urban route. The thermoelectric energy harvester was able to operate at temperature differentials as low as 6°C while supplying power to an onboard monitoring device in use. During testing, a phenomenon related to thermal imbalance between thermoelectric generators (TEGs) connected in series was observed. To investigate this effect, various electrical configurations were evaluated using two TEG units. The results indicated that, to prevent a negative impact on the net power output, the temperature differential of the lower-performing TEG must be at least 41.1% of that of the higher-performing unit.

DEDICATION

Para mi mamá y mi papá, muchas gracias por todo su apoyo, su amor, y por velar por mí para poder terminar mi carrera. Que dicha es tener su apoyo aquí y en el cielo, espero ser una buena ingeniera como ustedes. Para mis hermanos, Jesús y Dulce, muchas gracias por inspirarme en la ingeniería con sus propios caminos, ustedes me dieron mucho de donde elegir.

For my husband, Andres, thank you for being there through hardships and victories, I am so grateful that I have you in my life, I love you. And for my son, Jesus, everything I do is for you, te quiero mucho.

ACKNOWLEDGMENTS

First and foremost, I am sincerely grateful to my research advisor and professor, Dr. Constantine Tarawneh. I will never get to thank you enough for your support and the opportunities you gave us at the UTCRS center. It is not only your passion for your work but the commitment to our community that makes you one of my inspirations as an engineer.

I would like to thank Dr. Heinrich Foltz for your knowledge and patience. Whenever I needed help with my electrical engineering skills for this project, your support made a huge impact on my success. I would also like to extend my appreciation to Dr. Arturo Fuentes, whose involvement in my college journey ensured that I would be able to finish strongly.

I am also thankful to Dr. Brent Wilson, Mr. Byron Porter and Lee Cantu for giving me the opportunity to be a part of the Hum Industrial Technology team and develop more hands on skills as an engineer.

To my peers at the UTCRS center, thank you so much for helping me whenever I needed help, with wires or with machining. I am so grateful for your support and the chances you gave me to let me know each one of you. I wish you guys the best in your future!

This research was made possible through a partnership with Hum Industrial Technology, Inc., who provided financial and logistical support for the project. The work was also financially supported by the University Transportation Center for Railway Safety (UTCRS) through the USDOT UTC Program under Grant No. 69A3552348340.

TABLE OF CONTENTS

Page

LIST OF TABLES

Page

LIST OF FIGURES

Page

CHAPTER I

INTRODUCTION

Safeguarding the well-being of passengers, product transportation, and communities along train routes is a top priority in the rail industry. Despite major strides in improvements to safety, derailments still occur and lead to catastrophic results. According to the Federal Railroad Administration (FRA), a total of 663 derailments attributed to mechanical and electrical failures occurred nationwide between 2021 and 2024 [1]. Given that mechanical failures are a leading cause of these accidents, it is important to monitor the components that are the root cause. The demand for automatic and unmanned surveillance is finally able to be met due to advancements made in sensor technology.

1.1 Freight Component Health Monitoring Systems

The increase in the use of rail transportation can be attributed to the increased capacity to transport a large quantity of products across the country. Compared to alternative over-land transportation methods such as roadway or air transport, rail transportation has proven to be a more environmentally friendly [2] and often less cost-intensive alternative to the competing options. A variety of inspection techniques and technologies have been developed over the past century to monitor individual freight car components that have been recognized to be the most susceptible to failure, making them the catalysts for catastrophic derailments. Components such as bearings, axles, and wheels have been identified as undergoing most of the stress and wear during a rolling stock's operational lifetime. Studying and analyzing these stresses has provided insights for car owners to invest in updated component inspection methods, personnel training, maintenance, and parts renewal.

Condition monitoring devices were designed to surveil important aspects like the

components' temperature, vibrational signatures, and vehicle load, that could signal the initial degradation of these components. These devices aim to improve vehicle's performance efficiency, prolong the life of the components, and reduce potential service disruptions due to unnecessary and costly train stoppages or accidents. Condition monitoring devices have two categories: reactive and predictive systems. Reactive systems trigger an alarm when a part surpasses a predefined threshold and alerts the car owners that an immediate stoppage is required to avoid an accident, while predictive systems use algorithms to analyze data collected during service that could determine when to provide preventive maintenance.

1.1.1 Wayside Detection Systems

Wayside detection systems are fixed devices positioned along the railway track that gauge the health of the railcar's components as it passes by and alert the train operators when there are indications of component failure. They are classified as reactive systems since they cannot predict the future state of the parts and can only detect when failure is imminent. The most commonly used wayside detection systems are Hot Box (or Bearing) Detectors (HBDs) and Acoustic Bearing Detectors (ABDs), such as RailBAM and Trackside Acoustic Detection Systems (TADSTM).

Wayside HBDs are the most commonly used system for monitoring bearing health, with more than 6,000 units across the United States. HBDs use non-contact infrared (IR) sensors to scan the outer surface of bearing cups to obtain a dynamic bearing outer ring temperature and ambient temperature [3]. An alarm is triggered when the temperature difference between the bearing surface and the ambient temperature exceeds a predetermined threshold, indicating that the bearing needs to be removed from service to be inspected. Tarawneh et. al [3] performed laboratory and field tests to examine the efficacy of the HBDs. The results showed that they tend

to over or under predict values based on different physical characteristics of the components. IR sensors can fail to accurately detect the operating temperature due to several factors that include: cup degradation, heat-tinting, the location of the IR sensor relative to the bearing, and its simple one-point calibration procedure.

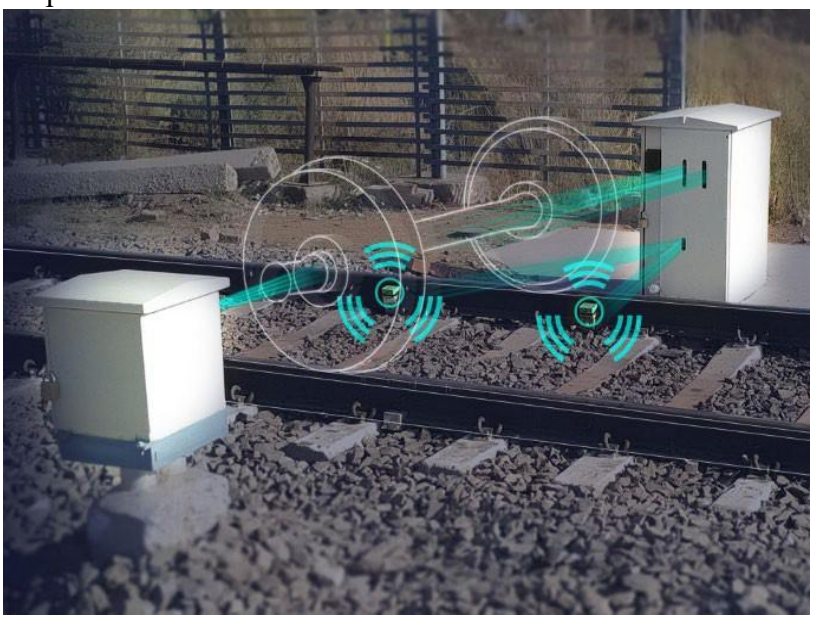

Figure 1: Hot Box/Bearing Detectors [4]

Underpredicted measurements or undetected defective bearings can lead to catastrophic accidents. A recent case highlighting the need for more effective condition monitoring technologies in freight rail operations was the derailment of Norfolk Southern train 32N, which occurred on February 3, 2023, in East Palestine, Ohio. According to the National Transportation Safety Board (NTSB), the probable cause of the derailment was an overheated bearing. The existing HBDs, failed to alert rail operators in a timely manner. As a result, the bearing reached a critical temperature, causing the axle to separate and subsequently leading to a derailment. The train was transporting hazardous chemicals, which ultimately contributed to a post-derailment fire [5].

Figure 2: Derailment of Norfolk Southern train 32N in East Palestine, Ohio. [6]

ABDs use wayside microphones to listen to the noise produced by the bearings on the passing rolling stock. The signal is analyzed and if there is a detectable bearing fault, it alerts the operator [7]. These devices may have the ability to become predictive systems; however, there are challenges such as noise interference from other subsystems of the vehicle and signal distortion due to the Doppler effect. According to a 2019 FRA report, there are currently 39 ABDs installed in North America [8], indicating that some vehicles may go their entire service life without passing through one of these detectors.

Figure 3: Trackside Acoustic Detector (TADS™) [9]

Figure 4: RailBAM Bearing Acoustic Monitor [10]

1.1.2 Onboard Monitoring Systems

Onboard condition monitoring systems are mounted on the vehicle and collect data while the rolling stock is in service. These condition monitoring systems allow for proactive maintenance because this approach tracks the life of the assets that may create catastrophic damage while in operation. The main benefit of onboard monitoring systems is the continuous or near continuous monitoring of components, whilst wayside monitoring systems only operate at their fixed location, which can be miles apart from one another. Thus, potentially allowing a defect to progress undetected between monitoring sites. Several onboard freight train bearing health monitoring systems have been introduced to the market such as the SMART-BOLT^{TM}, Timken Guardian^{TM} Bearing, Onboard Wireless Sensor Nodes (WSN), and the Hum Boomerang.

The SMART-BOLT^{TM} replaces a standard bearing end cap bolt at each end of the axle with a battery-powered thermal sensor that alerts the conductor when the temperature exceeds a threshold of 250 °F. Unfortunately, this system does not aid in the proactive maintenance of the vehicle because it does not track the bearing's condition over time [11].

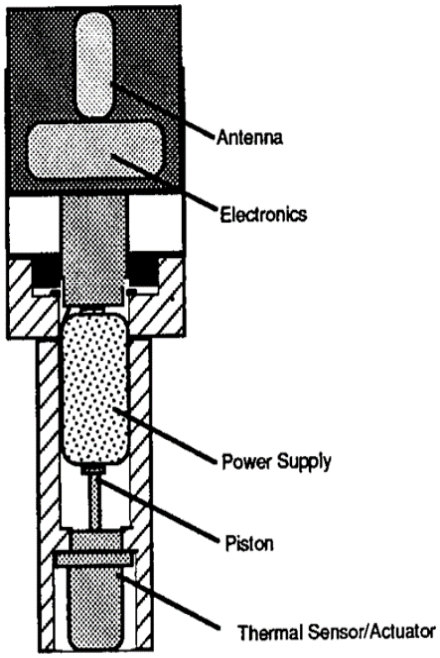

Figure 5: Diagram of SMART-BOLT™ [11]

The Timken Guardian™ bearing is outfitted with sensors that monitor the bearings, adjacent wheels, truck, and brakes. Features of the Timken Guardian™ include a 12-volt battery charged by an electric generator capable of providing up to 24 watts of power, and a microprocessor that collects and transmits data. Although this system is a good example of bearing condition monitoring with potential for proactive maintenance, the system can cause delays during disassembly and inspection due to the need of replacing the entire bearing in addition to being high cost [12].

Onboard Wireless Sensor Nodes (WSN) are a system of sensors, motes, and a locomotive gateway that provides real-time data and data transmission from individual sensors. It can provide early indications for train operators and train owners. However, this system only records real-time operating bearing temperature by mounting their motes on the railcars [13]. High bearing temperature may be considered as a last sign of imminent bearing failure.

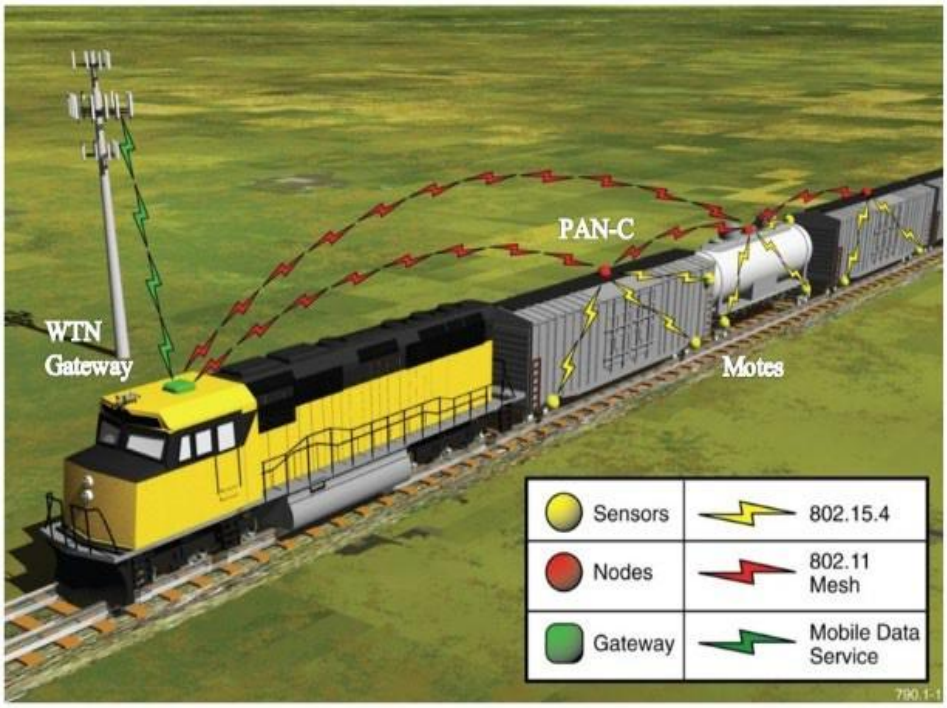

Figure 6: Onboard Wireless Sensor Nodes (WSN) [13]

The Hum Boomerang is a device mounted on the railcar bearing adapter, with sensors that monitor the vibration responses of the bearing, wheel, and track as well as the bearing temperature. It comes with a microprocessor that collects and transmits data wirelessly to a locomotive gateway. This system was developed by Hum Industrial Technology Inc., in collaboration with the University Transportation Center for Railway Safety (UTCRS) at UTRGV. The real-time data is analyzed, then sent to the train operator and car owners where they can take preventive measures regarding the components and prepare for maintenance. The system is equipped with batteries intended to enable continuous monitoring, however, because of this feature batteries can only last up to two years without replacement.

Figure 7: Hum Boomerang [14]

1.2 Motivation

One of the main challenges for adopting onboard monitoring systems is the unavailability of electric power on the bogies on which these systems are mounted. Simple solutions such as batteries have been suggested before. If used continuously, they will not last more than two years, adding another component to replace, and potentially causing service delays and costly disruptions. The use of finite duration electricity sources impedes technologies that could detect trends in bearing deterioration, therefore, it is essential to develop a reliable power generation method to sustain constant monitoring of train component health. A freight train can run routes lasting more than 12 hours, passing through miles of unpopulated areas, which make it impossible to recharge manually during operation. However, railcars experience forces such as vibration, hot temperatures, sun exposure, fast wind streams from the traveling train, etc., that can be harvested and transformed into energy that can power the onboard sensors.

1.3 Energy Harvesting Methods

Although most industries choose to use batteries for their ease of use and cost-effectiveness, they are not reliable as the sole source of power for this application. Life expectancy for continuous operation should exceed 5 years, but batteries have a finite supply of power and cannot meet this requirement without supplemental power source. Most railroads would not rely on technicians to service batteries for onboard sensors as it would add to the maintenance procedure and cost. Energy harvesting is a promising technique that can reuse energy from sources considered "waste" energy during mechanical and electrical processes. Energy harvesting typically exploits kinetic, thermal, solar, or electromagnetic sources [16]. To select an efficient and dependable energy harvesting system to power railroad onboard sensors, it must withstand the rough environment that is the service of rolling stock and be able to maximize the ambient energy to provide the required electrical power for the system. Energy harvesting refers to situations where the ambient energy sources are well-characterized and regular [15]. Systems such as solar and wind energy harvesters provide a high-power output, however, energy sources like vibration, thermal, magnetic field, and acoustic energy are more suitable for real-time monitoring sensors as they are always present during train operation. Vibration-based, photovoltaic, and thermoelectric energy harvesting methods have been previously studied for rail service.

1.3.1 Solar Energy Harvesting

Solar energy is a vast renewable source that surrounds the train and can supply an energy harvester mature enough to deliver electrical energy to low-power modules. The sun's energy can be transformed into electricity by a photovoltaic effect. When light hits a semiconductor

surface, it absorbs energy from the photons and freeing electrons, producing an electric charge. Although solar energy is more likely to be found supplying power to trackside components such as railroad crossing lights, station rooftops, and track health monitoring sensors [17][18], solar energy has the potential to supply power to onboard devices. Cii et al. [19] fabricated a solar panel system to feed an individual Wireless Sensor Node for a Wireless Sensor Network. The system was set up on the axle-box and took 1 month to completely charge the node during standard working operation considering night and day cycles. Vasisht et al [20] conducted an experiment by mounting photovoltaic modules on the rooftop of a rail couch of the Indian Railways. It was able to generate 1.3kWh of electricity a day. Even though solar energy harvesters range from high-power to low-power there is unpredictability influenced by the weather, solar panel positioning (shade and cell fragility), dust, and nights.

1.3.2 Piezoelectric Energy Harvesting

Piezoelectric harvesters have been considered for use in the rail industry due to their ability to transform mechanical energy into electrical power. This type of electricity is produced because of strain caused by mechanical energy applied to a material affecting their crystal structure, which creates polarization that generates current. A piezoelectric energy harvester made by Dziadak et al. [21] was able to generate 60.5 μW to power a WSN node with a range of vibrations from 4 to 6 Hz (at speeds of 50 km/h and 90 km/h). It is estimated that the harvester along with a 3.7V lithium battery will allow the WSN node to be powered for 13 years. This harvester operated below its resonant frequency as resonance may cause excessive stress that could potentially shatter piezoelectric devices. Piezoelectric harvesters provide insufficient power supply, poor durability and robustness for harsh environments experienced by rolling stock sensors. Shan et. al [22] proposes to optimize the mechanical transformer of a piezoelectric

energy harvester to maximize the energy transmission efficiency without surpassing fatigue limits. During experiments, the piezo stack energy harvester was able to provide 7.3mW at a measured railway track vibration signal. Whilst current state-of-the-art vibration harvesters generate hundreds of microwatts.

1.3.3 Electromagnetic Energy Harvesting

This type of energy is produced by the relative movement between a conductor and a magnetic field as described by Faraday's law of induction. Because of different structures there are three types of electromagnetic harvesters: direct voice-coil, spring resonance, and magnetic suspension [23]. There have been harvesters installed on the railway track that have been able to produce enough power for track-side devices such as Ling et al.'s [24] improved energy harvester. By a single-shaft Mechanical Motion Rectifier (MMR) which was able to generate over 10 W on average under 1 Hz and 5 mm sinusoidal excitation. Usually the onboard electromagnetic energy harvesters are designed for suspension systems of vehicle bodies. Pasquale et al. [25] proposed an onboard magnetic levitated generator with one fixed magnet on the base of the frame. 100 mW were obtained under the vibrations of a simplified coach at 80 km/h. A challenge that these harvesters may present are large impact forces caused by irregular vibrations during service.

1.3.4 Thermoelectric Energy Harvesting

Thermoelectric energy harvesting works on the Seebeck effect, an energy transformation process where an electric potential is generated due to a temperature differential between two faces of a semiconductor material. The voltage produced by the thermoelectric generators (TEGs) is proportional to the temperature gradient across the faces of the TEG. The performance of the thermoelectric devices depends on the Seebeck coefficient, electrical conductivity, thermal

conductivity, and thermal stability.

The components of a thermoelectric energy harvester are considered environmentally safe, silent, have a simple structure, and require minimum maintenance. Their main challenge is that they need to have a big temperature difference to produce high voltage.

Although the uses of thermoelectricity in the railway industry are not common, there are promising experiments in the automotive industry [26,27]. Ahn and Choi were able to generate 19.2 mW of power from a thermoelectric energy harvester on a high-speed train by utilizing a thermoelectric module and cooling fins, that were installed on the axle bearings' housing [28].

1.3.5 Energy Harvesting System Selection

To implement an onboard energy harvester to feed a continuous monitoring system it must have the following characteristics: sustain the rough environment that the freight rail is in, the ability to maximize the power generation from a well-characterized source, be independent of weather conditions, and must have adaptability to be universally fitted on multiple railcar designs. Ideally, this energy harvester is intended to support the adoption of continuous monitoring systems. Consequently, the system must be suitable for large-scale manufacturing, incorporating cost-efficient components and little to no maintenance of the system to ensure cost effectiveness.

Thermoelectric energy harvesting was selected because it best fits the outlined criteria. As previously mentioned, thermoelectric generators (TEGs) are considered environmentally safe, they do not have moving parts, they are silent, possess a simple structure and are easy to install. Additionally, prior research conducted at the University Transportation Center for Railway Safety (UTCRS) at UTRGV has demonstrated the effectiveness of thermoelectric energy harvesting for supplying power to a bearing health condition monitoring device. However, the

prototype experienced design limitations that could affect its performance during freight rail service. Possible solutions and optimization of the prototype will be further discussed in Chapter II.

CHAPTER II

UTCRS THERMOELECTRIC ENERGY HARVESTER

The prototype presented in this study builds upon the previous work done on a thermoelectric energy harvester device by Amaro [29]. The prototype developed at the University Transportation Center for Railway Safety (UTCRS) at UTRGV will provide energy to a low-powered onboard wireless bearing health monitoring device. The device was originally powered by a 3.7-Volt lithium-ion battery, however with the continuous monitoring feature this will decrease the battery's expected lifespan. Amaro's experimental results demonstrated the feasibility of utilizing a thermoelectric energy harvester to power a wireless monitoring device during freight train operations. Nevertheless, during experimental testing, it was discovered that the temperature gradient typically observed along standard routes was insufficient to meet the self-start voltage threshold of 0.9-Volt required by this energy harvester's iteration. This study will focus on optimizing the UTCRS thermoelectric energy harvester to supply power on similar standard routes.

2.1 Design considerations

Based on the Seebeck effect the thermoelectric energy harvester needs a heat and cooling source in order to produce power. The amount of energy harvested is proportionally related to the temperature difference between the heat and the cooling source. The heat source selected will be from the railcar bearing adapter and the cooling source will be the airstream forced convection generated by the train during travel.

2.1.1 Thermoelectric Generators

The thermoelectric generators (TEGs) are the semiconductor devices that will transform the temperature difference between the faces of the TEG to electrical power output. The TEGs

selected for this prototype were the Tecteg TEG2-126LDT (40×40 mm) scavenger model, which is designed and manufactured specifically for converting low temperature gradients. The module has Bi_2Te_3 (bismuth telluride) based p- (positive) and n- (negative) type semiconductors with opposite charge carriers, surfaces that are made of ceramic substrate with an outside layer of high thermal conductivity graphite sheets. In order to obtain the best temperature difference, the TEGs will be positioned on the leading and trailing faces of the railcar bearing adapter. These surfaces transmit heat through conduction from contact with the bearing cup which generates frictional heating from its rotational motion.

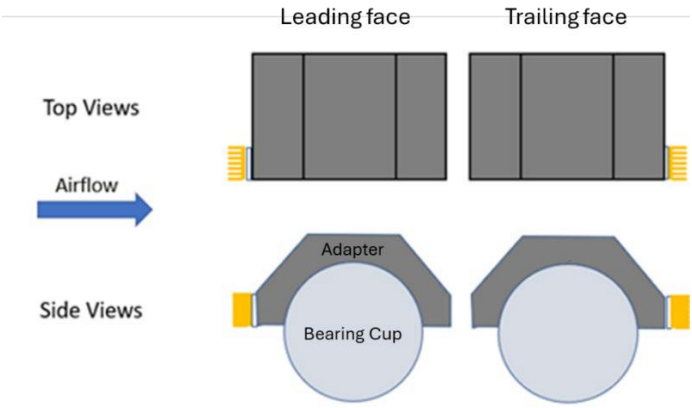

Figure 8: Thermoelectric energy harvester positioned on leading and trailing faces of railcar bearing adapter

2.1.2 Heat Sinks

The 6063-T5 aluminum plate-type heat sinks, with a thermal conductivity of 201 $\frac{W}{m \cdot k}$ were used to dissipate the heat from the cold side of the TEGs and create a temperature difference from the hot side. The heat are pressure mounted on the leading and trailing faces with the TEGs placed between the surface of the railcar bearing adapter and the heat sinks' base. For laboratory experiments a thermal grease with a thermal conductivity of 1.93 $\frac{W}{m \cdot k}$ was applied on the TEGs

cold and hot labeled sides to avoid any thermal resistance due to air pockets created from the metal surfaces to obtain optimal performance from the energy harvester.

2.2 Electrical Components

Based on Amaro's previous iteration of the thermoelectric energy harvester prototype, further enhancements to electrical components were necessary to enable reliable operation under low temperature gradient conditions. The energy harvester block diagram, as illustrated in Figure 9, shows key components from the previous iteration such as the boost converter and the Battery Management Chip (BMC) which were replaced by the single unit of E-Peas AEM20940. Additionally, the system's energy storing element was replaced by substituting rechargeable batteries for supercapacitors.

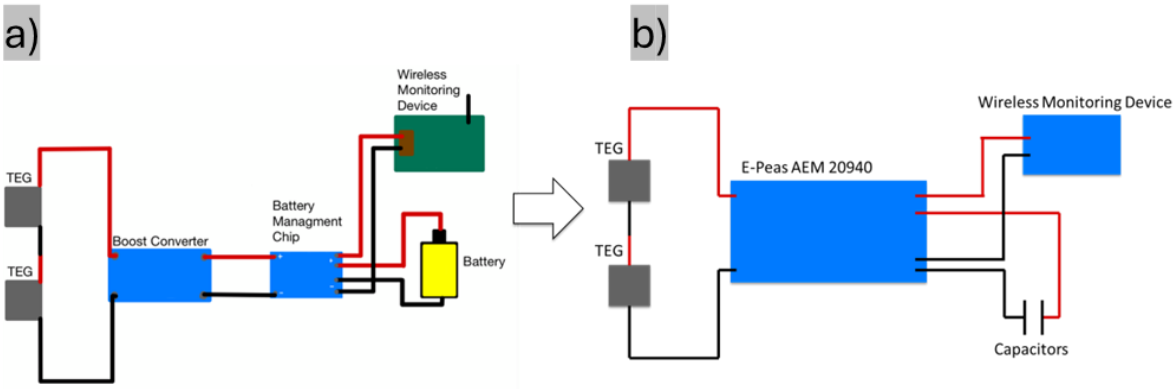

Figure 9: a) Block diagram of previous iteration of thermoelectric energy harvester and b) block diagram of latest iteration of thermoelectric energy harvester

2.2.1 E-Peas AEM20940

The E-Peas AEM20940 is an integrated energy management subsystem that is specifically designed for thermal energy harvesting. It enables the extension of battery life for a wide range of applications such as industrial monitoring, home automation, and smart agriculture. It simultaneously extracts DC power from the TEGs and recharges the selected energy storing element. The E-Peas AEM20940 can harvest available current up to 110 mA and it contains a boost converter, a BMC and a Maximum Power Point Tracker (MMPT) integrated.

Maximum Power Point (MPP) is a combination of voltage and current that yields the highest power output for the energy harvester. The MPPT is used to adjust to the variating operating conditions to continuously operate at the MPP of the device. The MPPT control circuit periodically measures the open-circuit voltage of the harvester to define the optimal regulation voltage.

The integrated boost converter raises the voltage available to a level suitable for charging the storage element in the range of 2.2V to 4.5V, depending on the system configuration. The E-Peas AEM20940 has a cold-start voltage of 0.38V, whereas the previous boost converter component used for this energy harvester had a minimum input voltage of 0.9V.

The AEM20940 has the option to include an external battery source and use it as the primary battery in case the storage element is depleted. The wireless monitoring system used to perform experiments in this thesis comes with two 1.5V Lithium AA batteries.

2.2.2 Energy Storing Element

In order to store the energy harvested, two 3V 50F Kyocera supercapacitors connected in series were selected. In the previous iteration, the thermoelectric energy harvester used a 14500 lithium-ion rechargeable battery as the energy storing element. Although both elements can

function as energy reservoirs, they do it by different means and are ultimately selected by their application. Supercapacitors store energy through distributing charged particles on two plates separated by an electrolyte and a thin insulator to create a potential difference. Batteries convert chemical energy to provide a static electrical charge for power. The supercapacitors have charging rates faster than the batteries and are able to release energy within seconds. One of the main differences between the batteries and the supercapacitors is their lifespan, usually 14500 batteries can last between 300 to 500 charge cycles, while the chosen supercapacitors have 500,000 cycles.

While both storing elements achieve the goal of replacing conventional batteries for onboard bearing health monitoring, the supercapacitors were ultimately selected due to the foreseen ability to withstand multiple charge cycles during freight rail service.

2.3 Electrical Array Configurations

During field operations the thermoelectric energy harvester may present with different temperature gradients on the leading and trailing side due to the airstream flow created by the direction of travel. The power output of the harvester is directly proportional to the temperature gradient as previously mentioned due to the Seebeck effect, however, when the TEGs are connected electrically in series with contrasting temperature differences for each component, they may experience power losses. Montecucco [24] explained that the thermal imbalance in the TEG array can impact the power produced by the Peltier effect. Contrary to the Seebeck phenomenon, it transports heat from one side of the TEG to the other when a voltage is applied. When two TEGs units are connected electrically in series or parallel array, the unit with the higher temperature differential ΔT_{Hi} may drive the unit with a lower temperature gradient ΔT_{Lo} to act as a Peltier cooler and consume some of the power generated. The following studies were

based on the impact of thermal imbalance between units by Capitanachi et al. [31].

In the analysis of a simple TEG unit at a moderate temperature gradient ΔT, as seen in Figure 10, the TEG can be represented by a Thevenin source with Open Circuit Voltage (V_{oc}) that is directly proportional to ΔT.

$$V_{oc} = k\Delta T \tag{1}$$

Where the factor k and the equivalent resistance R_{Th} is the same for both units and constant.

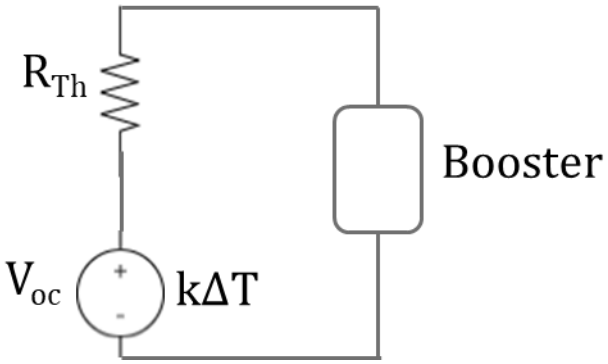

Figure 10: Schematic of the thermoelectric generator and a boost converter

The average power for the TEG during operation can be represented by a variation of Ohm's Law

$$P_{avg} = \frac{V^2}{R} \tag{2}$$

Substituting the voltage by $V = \frac{V_{oc}}{2}$, this is the midpoint where the maximum power occurs and the optimum resistance that is R_{Th} into Equation (2), obtaining:

$$P_{avg} = \frac{{V_{oc}}^2}{4R_{Th}} \tag{3}$$

Equation (3) represents the average power obtained by a single TEG with a moderate ΔT. When operating with a dual system of TEGs with the same ΔT, the diagram can be illustrated by

Figure 11, and the power average obtained can be represented by Equation (4):

$$P_{avg} = \frac{{V_{oc}}^2}{2R_{Th}} \tag{4}$$

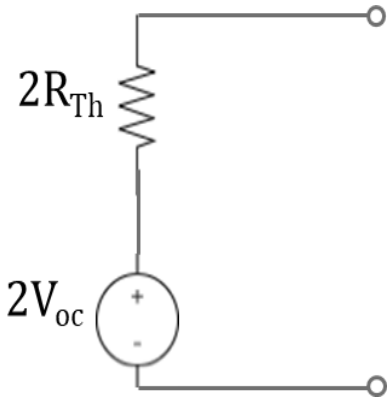

Figure 11: Simplified schematic of two TEGs operating electrically in series

However, considering a scenario where the temperature differentials are not the same for each unit, the schematic depicted in Figure 11, will be represented as shown in Figure 12.

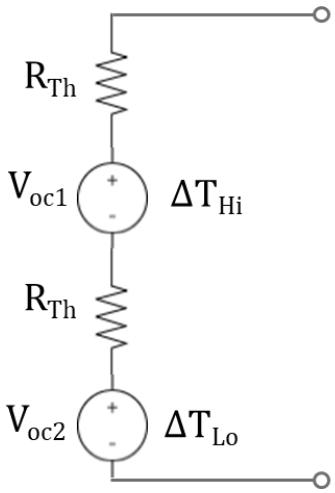

Figure 12: Schematic of TEGs operating at different temperature differentials in a series array

Under these circumstances, the open circuit voltage of the lower differential TEG, V_{oc2}, is substituted by the open circuit voltage of the higher unit, V_{oc1} along with the ratio of the temperature differentials between units.

$$V_{oc2} = V_{oc1} \frac{\Delta T_{Lo}}{\Delta T_{Hi}} = \alpha V_{oc1} \tag{5}$$

Substituting the values of this scenario into Equation (3) to obtain the power average, the result is:

$$P_{avg} = \frac{\left((1+\alpha)V_{oc}\right)^2}{4(2R_{Th})} = \frac{(1+\alpha)^2 {V_{oc}}^2}{8R_{Th}} \tag{6}$$

$$\text{when } \alpha < 1 \approx \frac{\Delta T_{Lo}}{\Delta T_{Hi}}$$

Analyzing these parameters facilitates the identification of conditions under which the optimal solution may be the system solely working from a single TEG, as determined through a comparison between Equation (6) and Equation (3):

$$\frac{(1+\alpha)^2 {V_{oc}}^2}{8R_{Th}} > \frac{{V_{oc}}^2}{4R_{Th}}$$

$$\alpha > \sqrt{2} - 1$$

In other words, if the temperature differential across the weaker TEG is less than 41.1% of the stronger TEG, its contribution to the net available power becomes negative. Under such conditions, it is more efficient to remove the weaker TEG from the circuit entirely. Boost converters have a minimum cold start threshold and if neither V_{oc1} nor V_{oc2}can reach, then both TEGs may be needed to be in a series array regardless of the effect of thermal imbalance between units.

The corresponding relationship is depicted in Figure 13. In the triangular region on the left, the combined open circuit voltages do not exceed the threshold voltage required to start the boost converter, then no power will be generated. Adjacent to the triangular region, neither TEG has enough voltage alone, however when combined, the open circuit voltage is sufficient to begin power generation. The other regions indicate where each unit will be more advantageous to use, only TEG 1, only TEG 2, or both in series.

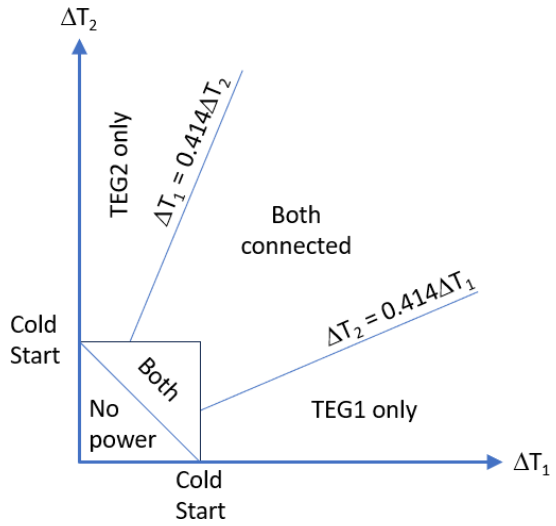

Figure 13: Operating regions for a combination of two TEGs in a series array at different temperature differentials

2.3.1 Preliminary Tests

To further understand the behavior of the TEGs under a thermal imbalance when connected in series a set of preliminary tests were conducted. First, a single TEG was used to execute a control experiment to compare the values obtained when the temperature is homogeneous. And secondly, a variation of configurations of TEGs connected in a series array were evaluated. The following tests were performed using a hotplate set at 50°C (122°F) as the heat source and a heatsink/cooling fan was used as the cooling source. To create the temperature mismatch between the TEGs, TEG 1 unit was placed between the hotplate and the heatsink/cooling fan, while TEG 2 was exposed to ambient conditions of the room at 21°C (70°F). The temperature differentials were selected to demonstrate the negative effects of having one TEG at significantly lower differential than the other unit.

The data was monitored and collected by digital measurement devices used to record the individual input TEG voltage, the TEG input current, and the voltage of the supercapacitors to

monitor the charge.

2.3.2 Single Thermoelectric Generator

A control experiment was conducted using a single TEG. Once a thermal steady state set at 50°C (122°F) was reached, the hot side of the TEG was placed directly on the hotplate and a heatsink/cooling fan was positioned on the cold side of the TEG. The objective of this experiment was to determine the maximum charge rate achievable by a TEG under conditions of thermal equilibrium.

The average charging rate is determined from the final stored energy of the capacitor.

$$U = \frac{1}{2}CV^2 \tag{7}$$

Where, U represents the final stored energy in the capacitor, C is the capacitance of the capacitor, and V is the voltage.

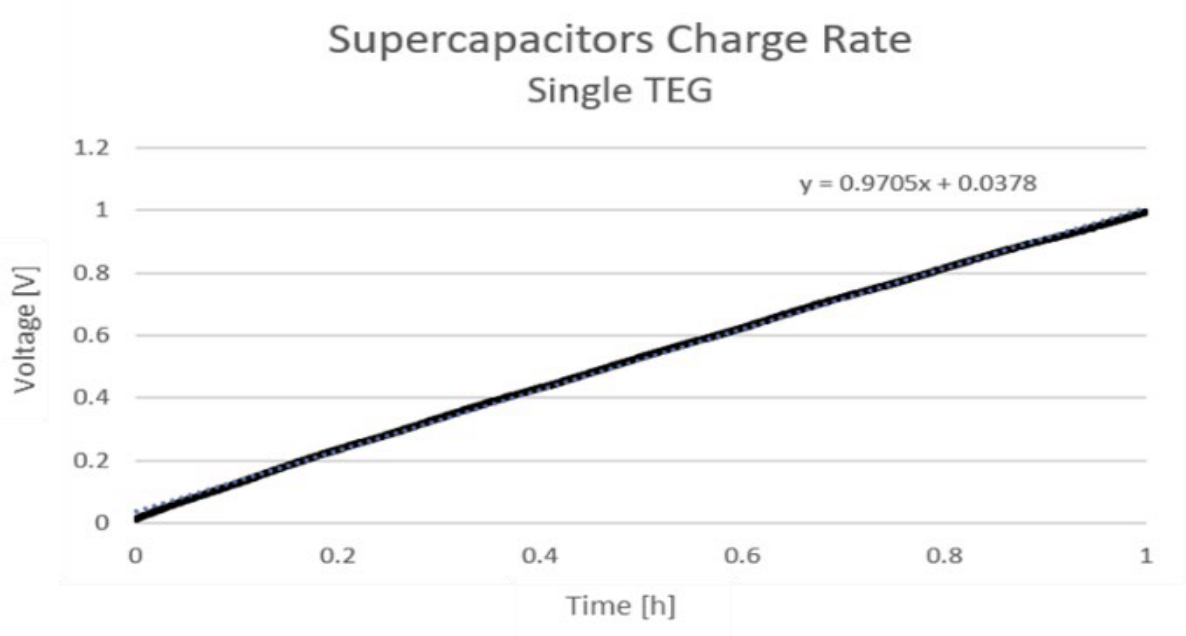

Figure 14: Supercapacitor charge rate of a single TEG

As shown in Figure 14, the solid line depicts the measured performance of the TEG

charging a supercapacitor for the lapse of an hour. The dotted line represents the average voltage gained per hour. The supercapacitor showed an initial gain of 0.97V and inputting the values of the experiment into Equation (7), a total energy of 12.13 Joules and charging power of 3.34 mW was harvested in the duration of the experiment.

2.3.3 Series Array Configuration

The first configuration tested was a simple series connection between both TEGs under the conditions previously mentioned in section 2.3.1. Figure 15 shows two TEGs with the output connected to a boost converter which will charge two supercapacitors.

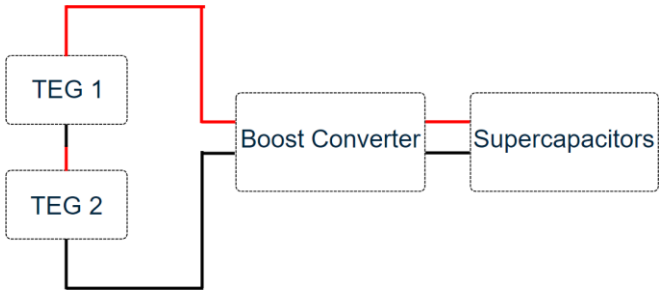

Figure 15: Block diagram of TEGs in a series array configuration

Figure 16 depicts the charging performance of the series array, with one TEG having a much higher temperature differential than the other unit. In this experiment, the supercapacitors gained a charge of 0.36V and the TEGs exhibited a charging power of 1.15 mW. There is a significant decrease in charge observed within the same one-hour time frame when compared to a single TEG.

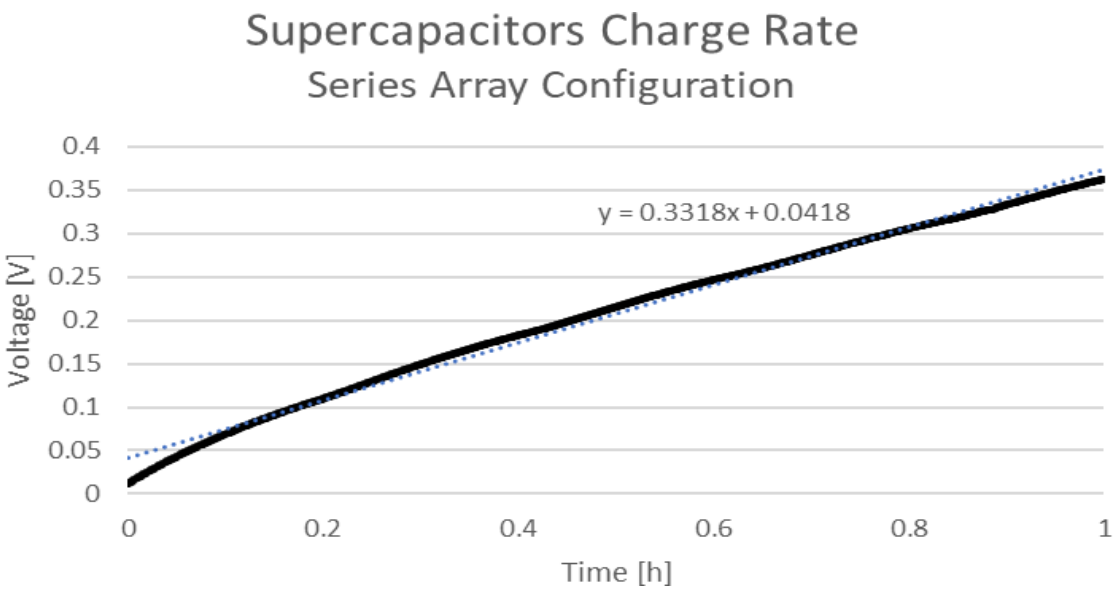

Figure 16: Supercapacitor charge rate of series array configuration

2.3.4 Series Array With Bypass Diode Configuration

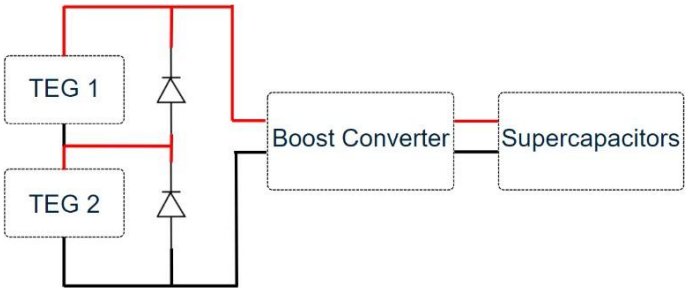

Figure 17: Block diagram of series array with a bypass diode configuration

In the configuration shown in Figure 17, the TEGs were still connected electrically in a series array with an additional diode connected in parallel with each TEG. The purpose of adding this diode was to mitigate some of the negative effects caused by having two TEGs without the same temperature differential. In this scenario, TEG 1, the unit with the highest temperature gradient, had its output connected to the boost converter, while TEG 2 was disregarded, with its current going through the diode instead. A limitation of this configuration is the voltage drop across the diode, which can be mitigated by using a diode with a low threshold voltage.

Figure 18 depicts the performance of the series array with bypass diode configuration, which had a potential energy output of 5.19 Joules and an average initial charging power of 1.44mW. This configuration showed improvement from the series array; however, it still underperformed as compared to the single TEG case.

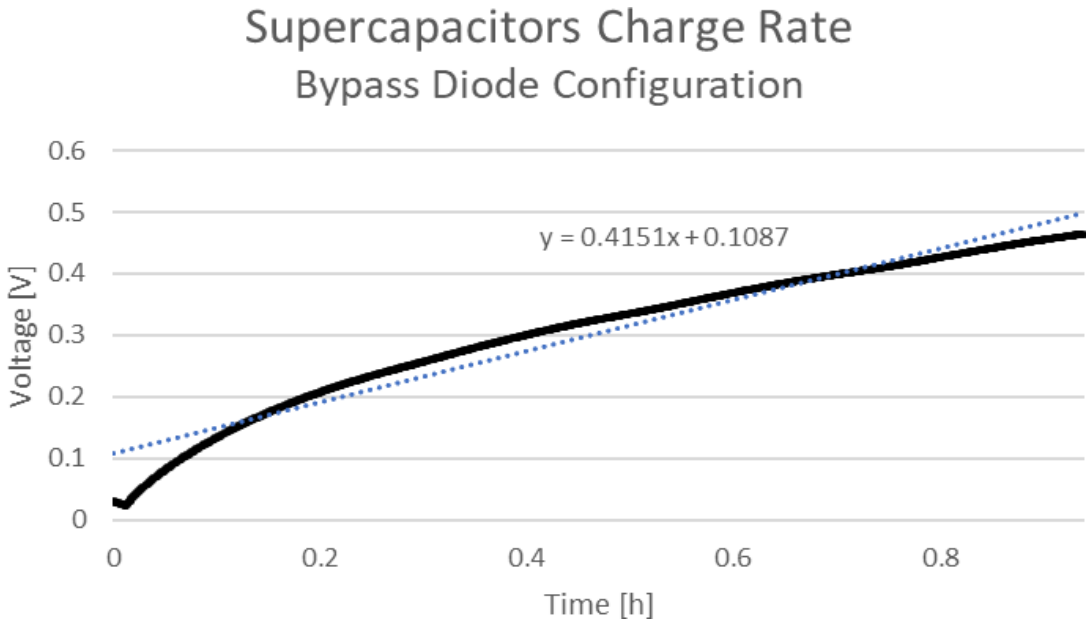

Figure 18: Supercapacitor charge rate of series array with bypass diode configuration

2.3.5 Isolated Thermoelectric Generators

In the configuration, shown in Figure 19, the TEGs were electrically isolated having their own boost converter unit with their outputs merged with the supercapacitors, with each boost converter having a superdiode added to its output to prevent backflow from each unit into the other. This system should be the most optimal variant since it completely negates all drawbacks from the thermal imbalance between TEGs connected in series. By isolating each TEG, both devices can supply the maximum amount of power harvested. Nevertheless, the challenge for this configuration was that each TEG had to surpass the cold start voltage of its respective boost

converter.

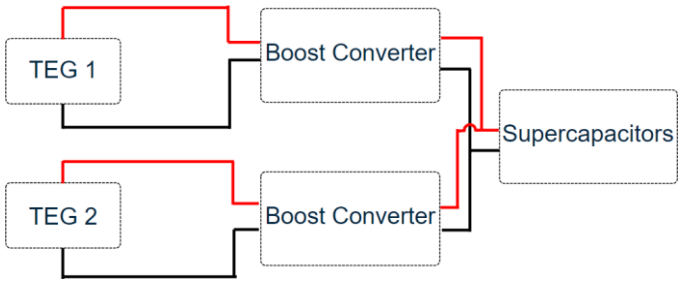

Figure 19: Block diagram of isolated TEGs configuration

Figure 20 illustrates the charging rate of the supercapacitors by the isolated TEGs. Over the duration of the test, this corresponds to the potential energy gain of 6.45 Joules and an initial charging power of 1.79 mW. Although this configuration should have had a closer outcome to the single TEG, it experienced a significant loss in the superdiode combining circuit. This configuration outperformed the simple diode bypass; albeit at the cost of increased complexity and parts count.

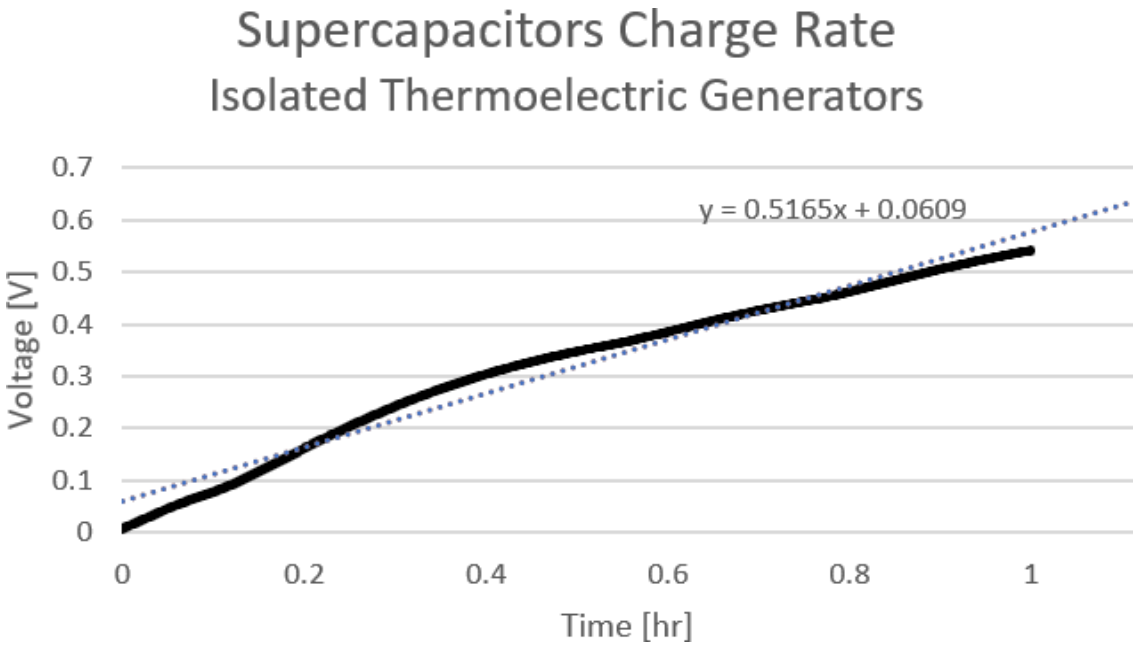

Figure 20: Supercapacitor charge rate of isolated TEGs configuration

2.3.6 Configuration Selection

When using thermoelectric energy harvesters in applications, it is inevitable to undergo

some thermal imbalance between units.

Although the single TEG is the system that showed a higher power output for thermal energy harvesting, having two TEGs in series is necessary for the application of powering an onboard monitoring system during freight rail service. Utilizing two TEGs enables the energy harvester to operate independently of the train's direction of travel, as the forced convection produced by the airstream creates a higher temperature difference for each TEG.

Figure 21 can be used to compare the power values obtained during the one-hour test with the conditions explained in section 2.3.1. The optimal series array was the isolated TEGs configuration by which outputted 1.79 mW compared to the simple series connection that outputted 1.15 mW. However, the independently boosted TEGs may not be cost effective and would depend on the individual performance of each TEG to achieve the cold start voltage of each boost converter. A simple bypass diode across each TEG can mitigate some of the power losses due to temperature differential mismatch, but although it outperformed the simple series connection the performance failed to meet the expectations of the single TEG output values. This testing demonstrated the need to consider more configurations to reduce the negative impact of thermal imbalance between TEGs, such as low voltage switching methods to disregard the lower performing unit when it negatively affects the whole system.

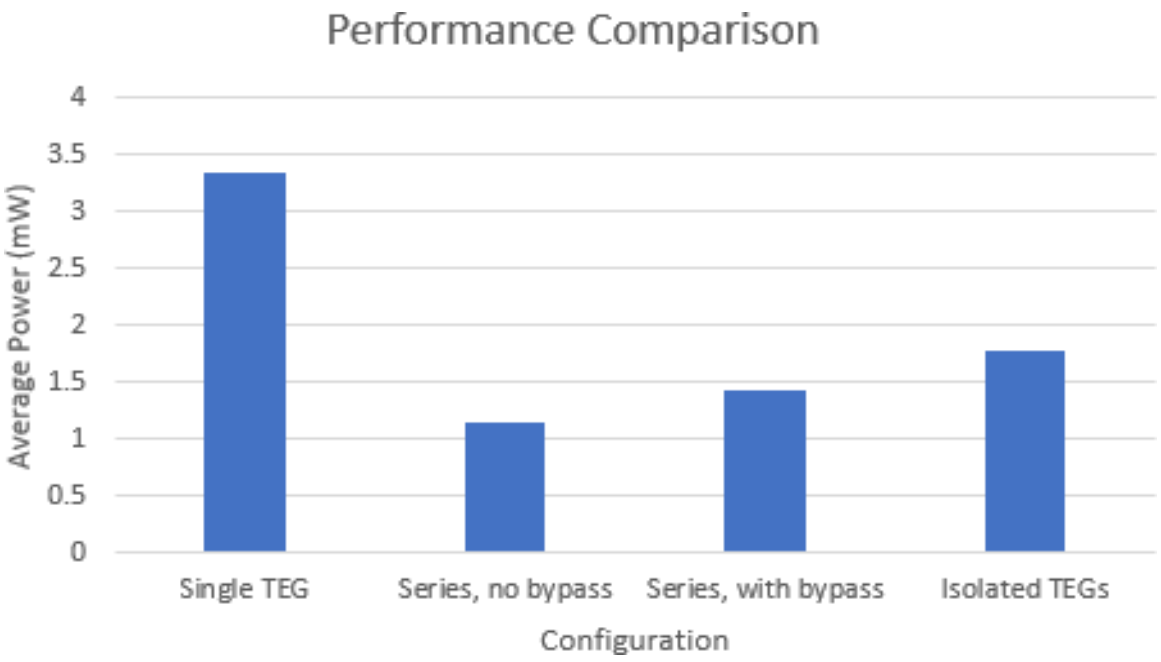

Figure 21: Supercapacitor charge rate comparison

CHAPTER III

EXPERIMENTAL SETUP AND PROCEDURES

To validate the modifications done on the thermoelectric energy harvester, the performance of the device was assessed while powering a wireless bearing monitoring device in a controlled laboratory setting.

3.1 Dynamic Bearing Test Rigs

For freight rail applications, the energy harvester must be able to withstand the harsh environment, be a universal fit on railcars and be able to maximize the energy source harvested. In order to predict the on-field performance of the thermoelectric energy harvester, bearing operating conditions for freight railcars were replicated. The controlled settings were achieved by using the UTCRS dynamic bearing test rigs located at the University of Texas Rio Grande Valley (UTRGV) facilities. The dynamic bearing test rigs simulate the parameters experienced by tapered roller bearings in freight rail service. The system is able to test four classes of railroad bearings classified by the Association of American Railroad (AAR) as seen in Table 1. For this study, AAR Class F bearings were used for all the laboratory experiments carried out.

Table 1: Bearing classes, dimension and load capacities according to the AAR

Bearing Class	Size [in.]	Load [kN]	Load [lbf]
Class E	6 × 11	117	26,300
Class F	6½ × 12	153	34,400
Class G	7 × 12	169	38,000
Class K	6½ × 9	153	34,400

The University Transportation Center for Railway Safety (UTCRS) possesses a Single Bearing Tester (SBT), pictured in Figure 22, a Four-Bearing Tester (4BT), shown in Figure 23a), and a Four-Bearing Chamber Tester (4BCT), depicted in Figure 23b). The bearing test rigs are outfitted with sensors that monitor temperature, vibration and load conditions.

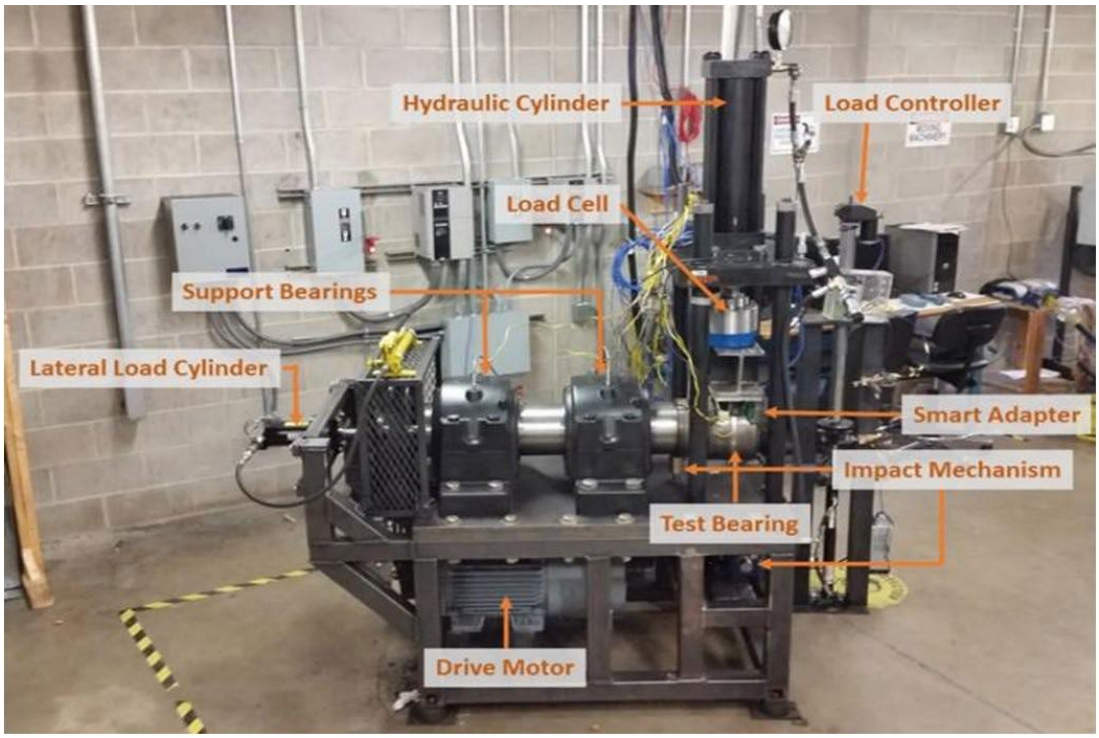

Figure 22: Single Bearing Dynamic Tester (SBT)

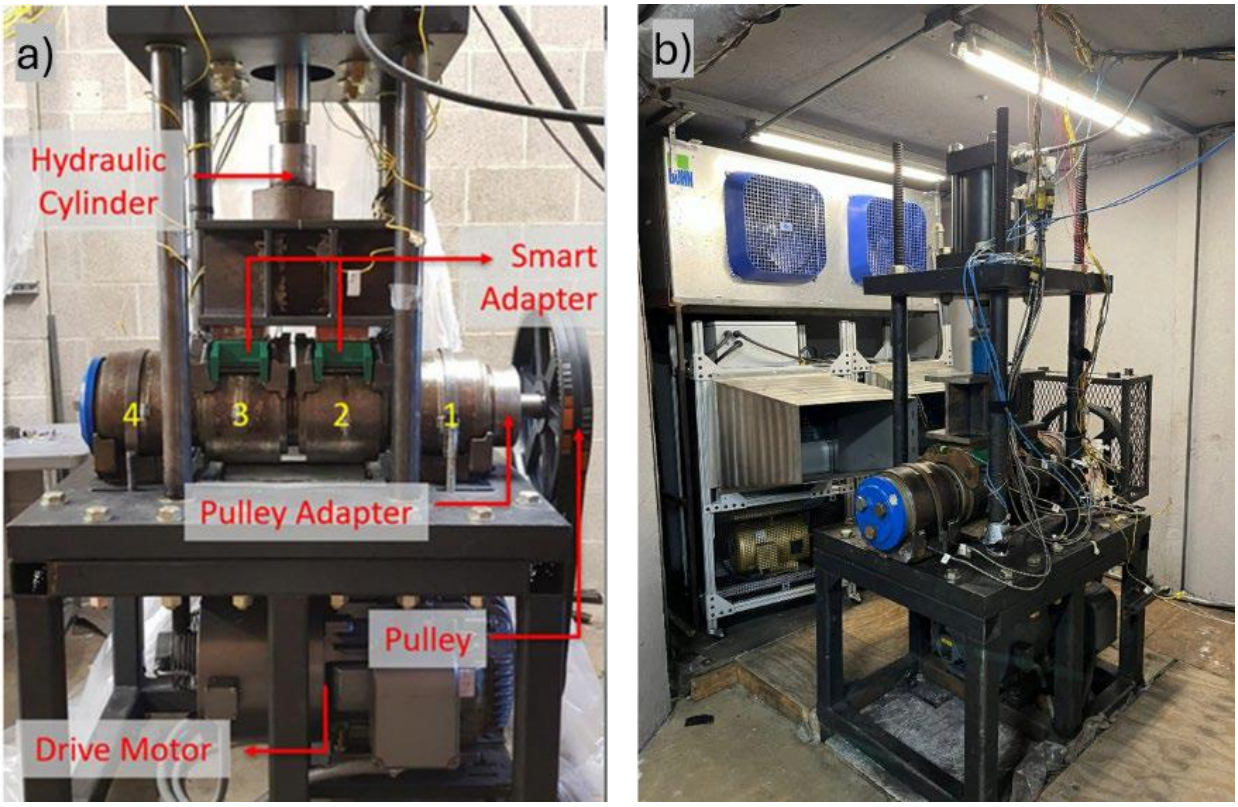

Figure 23: a) Four-Bearing Dynamic Tester (4BT) and b) Four-Bearing Chamber Dynamic Tester (4BCT)

The SBT simulates the conditions of a single railroad bearing mounted on the wheel-axle assembly of a freight railcar. While the 4BT and 4BCT can accommodate four railcar bearings at a time, these are positioned with two control bearings bottom-loaded while the two middle bearings being top-loaded, which are the ones used as test bearings because they are loaded like in field service. Both testers include industrial fans moving air perpendicular to the axis of the assembly providing passive air cooling of 6m/s (13.4 mph). Although the 4BCT is housed within an environmental chamber that is capable of maintaining a controlled ambient temperature in the range of -40 to 65 °C (-40 to 150 °F), the testing conducted for this study utilized a set ambient of 21°C (70 °F).

The tester rigs allow for precise control of loading conditions using load controllers that regulate a hydraulic cylinder to maintain a constant applied load on the bearings. The main scenarios studied included the 17% railcar load (i.e., a load of 26 kN or 5.85 kips per bearing) that represents an empty railcar, and 100% railcar load (i.e., a load of 153 kN or 34.4 kip per bearing) simulating a fully loaded railcar.

The bearing test rigs are also equipped with a 22 kW (30 hp) variable speed motor controlled with a variable frequency driver (VFD) that can provide angular axle speeds that mimic train traveling velocities of up to 137 km/h (85 mph).

3.2 Route Simulation Selection

Speed, load, and the condition of the bearing are major factors for the railcar bearing adapter temperature. With the ability to replicate train routes for testing development, a thermoelectric energy harvester prototype unit was mounted on an AAR Class F railcar bearing adapter to be tested on the UTCRS dynamic test rigs. In order to validate its performance, the harvester was tested under adverse conditions that could lead to low temperature gradients, to verify the efficacy of the new modifications of the unit.

The route selected simulated a roundtrip from Fairfield, AL to New Orleans, LA. This route models a freight railcar's journey transporting cargo from a steel mill to a shipyard, and it runs for 427.2 miles in length and 11.59 hours in duration. The speeds for this route were estimated by using the urban density of the corresponding area along with existing railroad data [32]. Figure 24 shows the map of the route and Table 2 lists the cities that the route intersects. The table also shows the distance between the cities and the simulated train speed conditions along with the time elapsed in travelling from one city to the other.

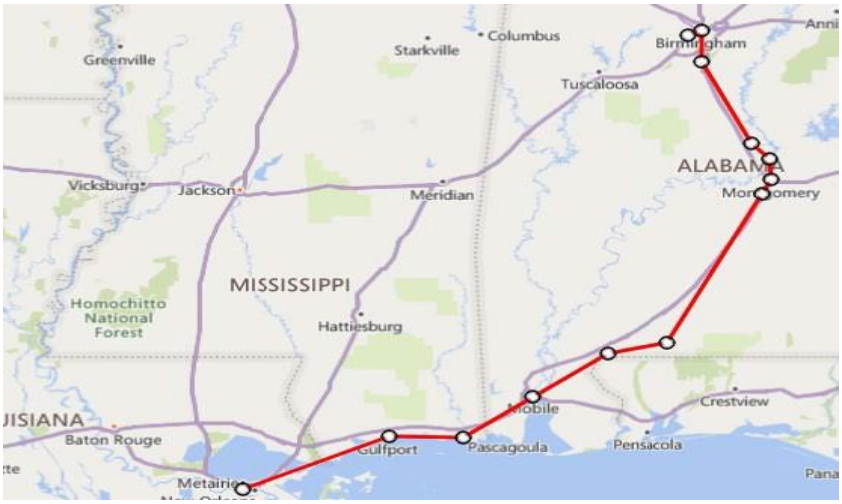

Figure 24: Map of route selected (Fairfield, AL to New Orleans, LA [32]

Table 2: List of cities along the route selected and speed limits (Fairfield, AL to New Orleans, LA)

City	Distance [mi]	Speed [mph]	Elapsed Time [h]
Fairfield	0.0	25	1.26
Pelham	31.5	35	1.52
Rollins	84.7	55	0.22
Elmore	96.8	35	0.33
Montgomery	108.4	25	0.36
McGehees	117.4	60	1.61
Brewton	214	55	0.51
Atmore	242.0	45	0.98
Mobile	286.1	35	2.11
Gulfport	360	25	2.69
New Orleans	427.2	25	0.0

This route is located in an urban area which requires lower speeds for longer periods of time, and for this particular study, can be considered as adverse conditions because it will have an impact on the temperature of the railcar bearing adapter. The thermoelectric energy harvester will need to be evaluated in this type of condition to determine if the amount of charge produced is sufficient to be able to harvest and operate a wireless bearing monitoring device.

3.2.1 Instrumentation Setup

The data was monitored and recorded using OWON B35T Multimeters following the diagram in Figure 25. It measured values every ten seconds during the experiments performed. The voltage of the leading and trailing TEGs was collected, as well as the input current to the wireless bearing monitoring device which has the E-Peas AEM 20940 embedded in its circuitry. Lastly the voltage of the capacitors was also monitored in order to confirm the harvester was producing a charge.

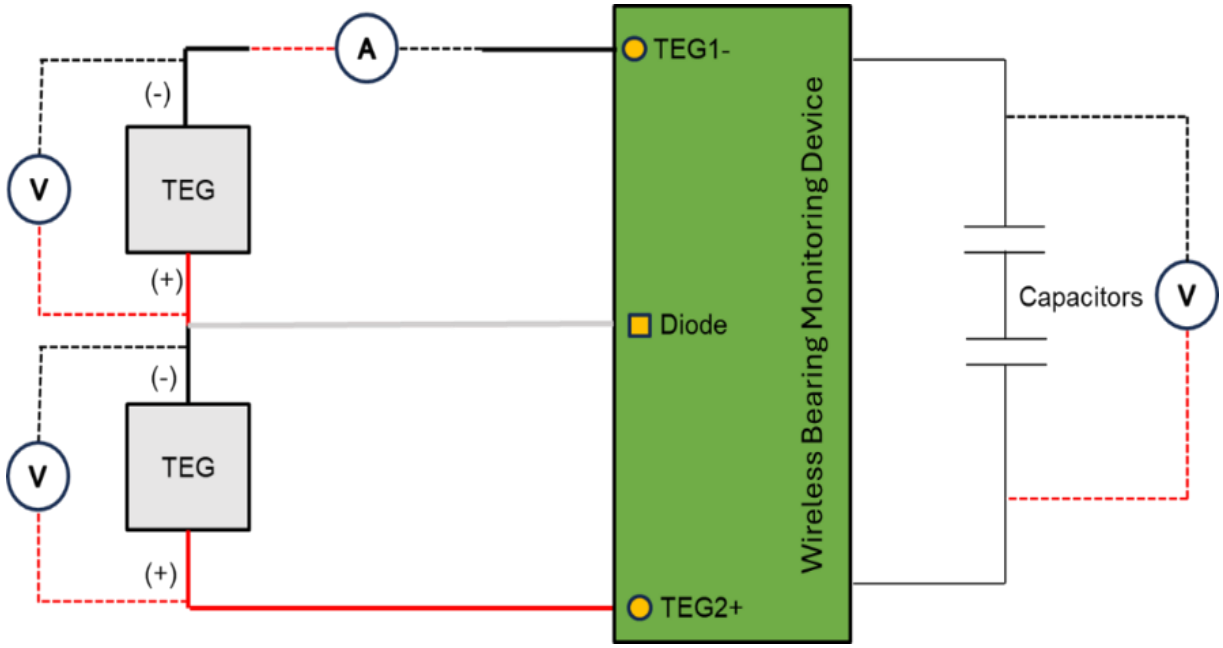

Figure 25: Diagram of setup to monitor values during laboratory experiments

CHAPTER IV

RESULTS OF SIMULATED ROUTE TESTING

The following experiments were conducted utilizing the four-bearing chamber tester (4BCT) with the air conditioning unit set to 21°C (70°F). The tester was fitted with four Class F bearings, including three defect-free control bearings and one defective bearing that developed a spall on the outer ring (cup) during operation. The bearings were positioned as shown in Figure 26, with the defective bearing (B3) placed in the middle along with a control bearing (B2). As previously mentioned, the bearings in the middle of the test axle configuration are top loaded to replicate field conditions.

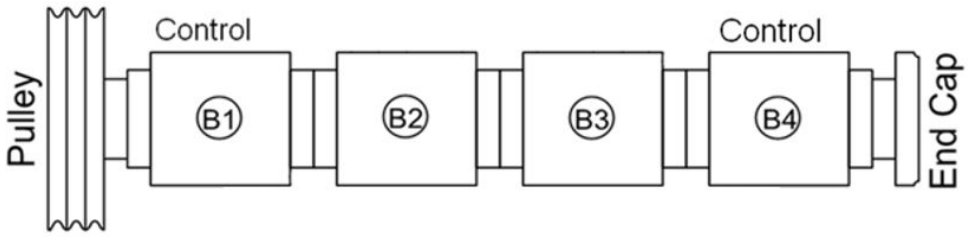

Figure 26: Test rig bearing schematic

Industrial fans were set perpendicular to the test rig with airflow speed of 6 $\frac{m}{s}$ (13.4 mph) to mimic the airstream created by the travelling train.

Two thermoelectric energy harvesting units were pressure mounted onto the leading and trailing faces of the railcar bearing adapter of the B3 bearing. These devices were electrically connected to an onboard bearing health monitoring device, which integrated the energy harvesting circuitry, as shown in Figure 27.

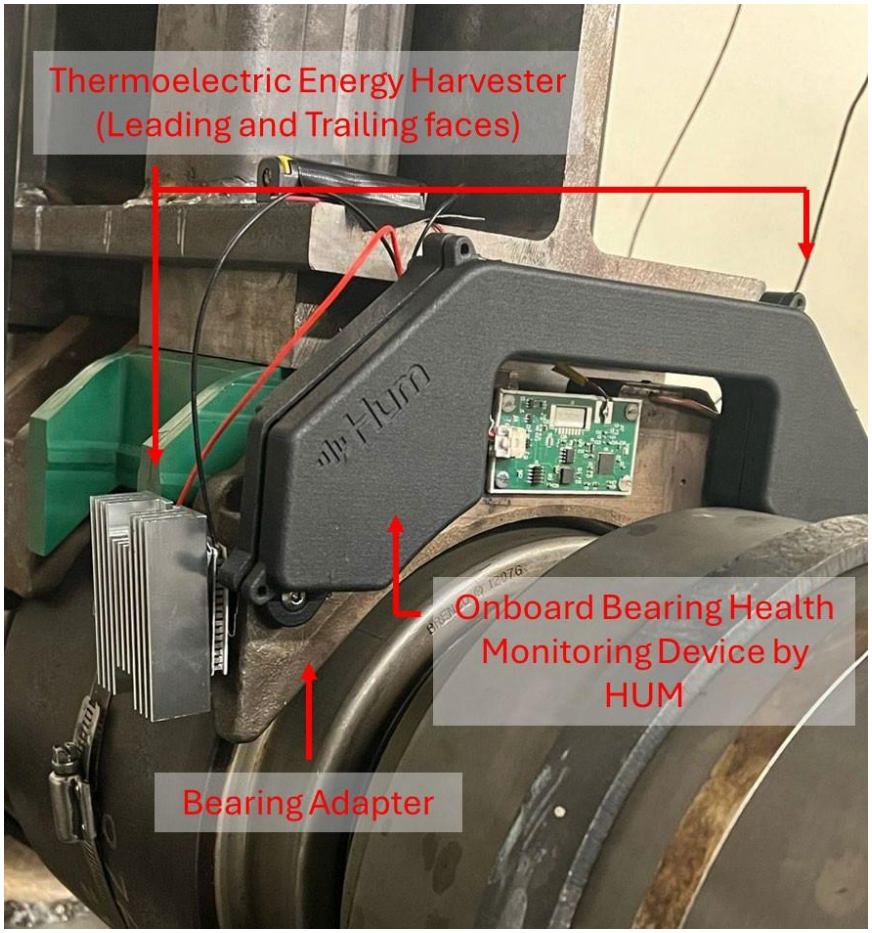

Figure 27: Thermoelectric energy harvester mounting on bearing adapter

4.1 Preliminary Tests of Standard Speeds

Preliminary tests were performed to analyze the thermoelectric energy harvester's performance under high and low speeds while supplying power to an operating onboard bearing health monitoring device. In the U.S. the Federal Railroad Administration (FRA) typically defines $129\ \frac{km}{h}$ (80 mph) as the upper limit for freight train speeds depending on the track's infrastructure and condition. However, actual operating speeds are typically lower due to factors such as equipment limitations, safety considerations, and industry practices. Even though the UTCRS test rig can achieve 80 mph, this experiment aimed to test realistic speeds that are encountered during service for trains on routes across urban and rural areas. The selected high speed was 80

$\frac{km}{h}$ (50 mph), whereas 40 $\frac{km}{h}$ (25 mph) was selected as a low speed, and each speed was tested under full load and empty railcar conditions. Temperature was acquired using K-type surface contact thermocouples that were placed at the base of the heat sinks and at the surface of the railcar bearing adapter. This setup was repeated on the leading and trailing faces where the energy harvesters were located without disrupting the contact with the railcar bearing adapter. Data was collected once the tester reached steady state operating conditions to maintain consistency in the results.

4.1.1 Experiment 280B – Unloaded (Empty) Railcar, Two Different Speeds

As explained before, the aim of this experiment was to quantify the amount of charge the energy harvesting could generate at different speeds and loads that are seen during field operations.

For the beginning of this test, the tester's speed was set to 40 $\frac{km}{h}$ (25 mph) with the condition of an empty railcar (17% railcar load). For the second part of this test, the speed was increased to 80 $\frac{km}{h}$ (50 mph) while maintaining the load conditions.

After the tester reached a thermal steady state, the temperature differentials of the surfaces of the adapter surface and the base of the heat sinks were obtained for each face. For the case of the high speed, the temperature differential was 6.6 °C (11.9°F) on the leading side and 5.8 °C (10.4°F) on the trailing side. Meanwhile for the low speed, the temperature differential was 4.3 °C (7.7°F) on the leading side and 3.8 °C (6.8°F) on the trailing side.

As shown in Figure 28, the total voltage gained for the high speed was 1.69 V and the total gain for the low speed was 0.406 V after a five-hour test. Inputting these values into Equation (7) from Chapter II, the average power obtained for each run was 1.993 mW for the

high speed and 0.113 mW for the low speed.

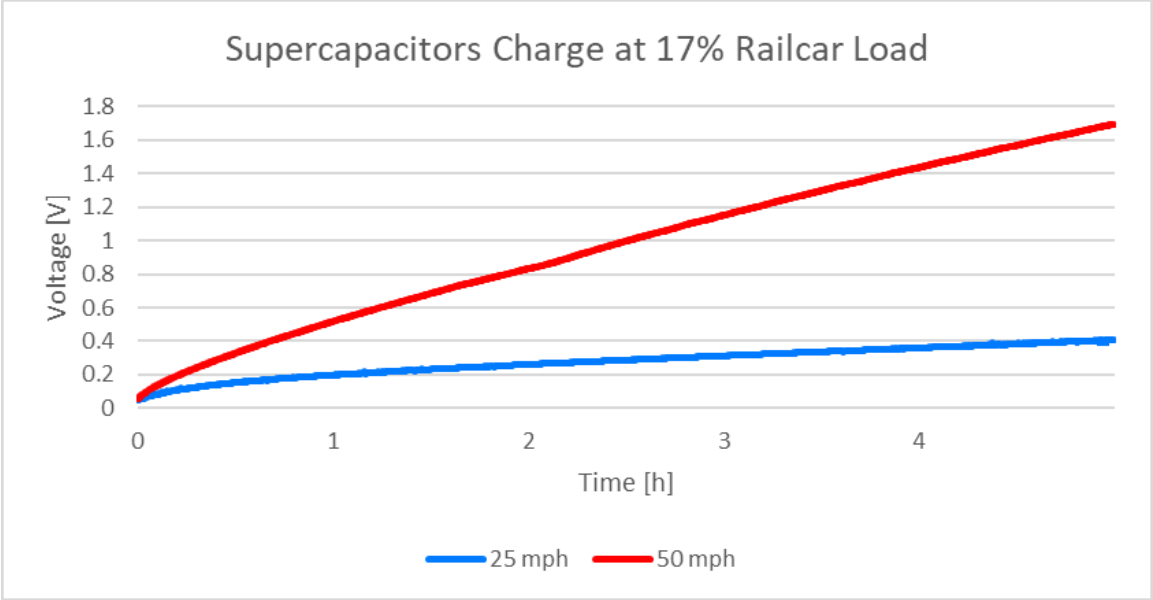

Figure 28: Supercapacitors charge rate at 17% railcar load with different speeds

4.1.2 Experiment 280B – Loaded Railcar, Two Different Speeds

Under high-speed conditions, the temperature differential measured 7.9°C (14.2°F) on the leading side and 6.9°C (12.4°F) on the trailing side. In contrast, under low speed conditions, the leading side exhibited a temperature differential of 5.6°C (10.1°F), while the trailing side measured 4.4°C (7.9°F). As shown in Figure 29, the total voltage generated for the high speed condition was 2.45 V and 0.65 V for the low speed. Calculating the corresponding average power output with Equation (7) for the high-speed condition was 4.19 mW and 0.29 mW for the low-speed.

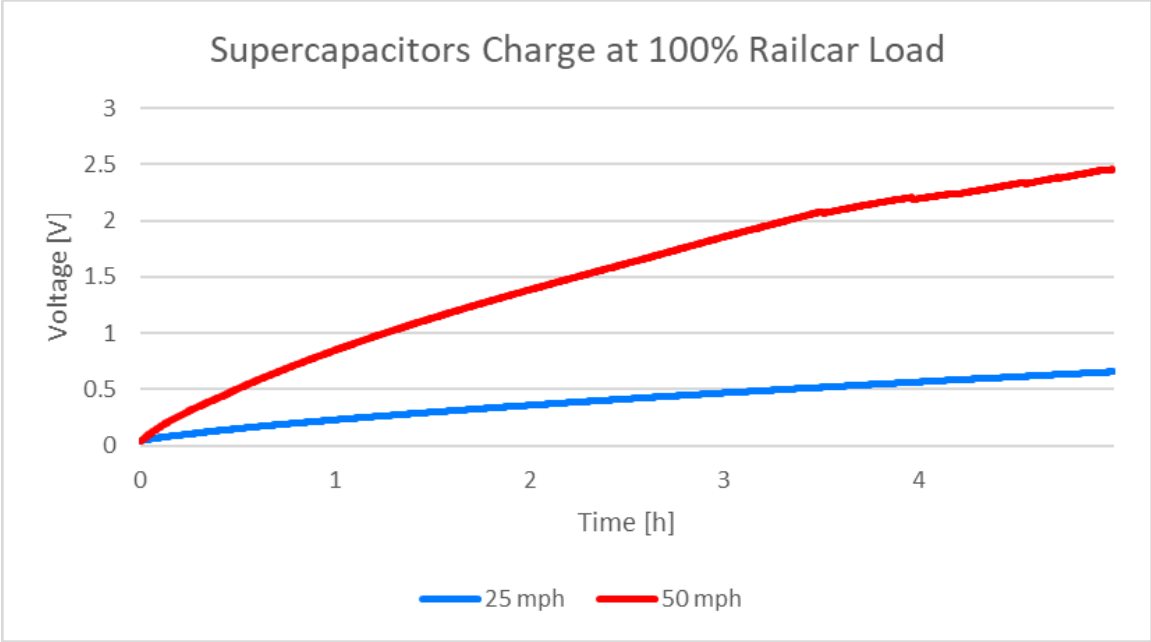

Figure 29: Supercapacitors charge at 100% railcar load with different speeds

As seen in both test scenarios, the temperature difference on the leading face of the railcar bearing adapter is higher than the trailing side. This can be potentially due to the direct exposure of the heat sinks on the leading face to the airstream, whereas the trailing face receives airflow after it has traversed around the adapter. The airstream is intended to simulate the airflow encountered by the travelling train; therefore, the observed temperature gradient is influenced by the direction of travel.

4.2 Full Route Testing

As previously mentioned, the route selected recreates a freight railcar transporting cargo from Fairfield, AL to New Orleans, LA. The purpose of this experiment was to validate the modifications done to the thermoelectric energy harvester and if there was improvement from the previous iteration. In route testing with previous thermoelectric energy harvester prototype, it was determined that during the selected route, the temperature difference was too low to meet the boost converter start voltage. This route may generate unfavorable operating conditions since the

route requires lower speeds for long periods of time, generating a low temperature gradient.

The following tables display the segment duration, simulated train speed, average ambient temperature ($Avg.\ T_{amb}$), temperature difference on the leading side ($\Delta T\ Leading$), temperature difference on the trailing side ($\Delta T\ Trailing$), TEG input current, the voltage charge produced, and the average power generated per segment. The last column in the table indicates the average power consumed by operating an onboard bearing health monitoring device communicating the bearing health status to the user.

4.2.1 Field Route Simulation – Loaded Railcar

Table 3 summarizes the data collected from the performance of the thermoelectric energy harvester on a fully loaded railcar. The generated power column corresponds to the power output at the specific speed, averaged over each time segment. For this case, the temperature differentials across the TEG modules increased with higher vehicle speeds. At the speed of $40.2\frac{km}{h}$ (25 mph), the system generated 0.19 mW, with a temperature differential of 3.4°C (6.1°F) on the leading side and of 3.2°C (5.8°F) on the trailing side.

In contrast, the highest power recorded was 3.9 mW at a speed of 72.4 $\frac{km}{h}$ (45 mph), corresponding to the temperature differentials of 7.4°C (13.3°F) on the leading side and 6.7°C (12.1°F) on the trailing side.

Over the duration of the test, the system exhibited an overall average power generation of 1.98 mW. Notably, the net voltage of the supercapacitors at the end of the test experienced a decrease, this can be attributed to the circuit's program that lets the system be fully powered by the energy harvester; prior to this threshold, the system operated using its primary batteries.

Table 3: Results of thermoelectric energy harvester performance for the simulated field route at 100% railcar load – Defective bearing

Time [h]	Speed [rpm]/[mph]	Avg. T_{amb} [°C]	ΔT Leading [°C]	ΔT Trailing [°C]	Charge Current Produced [mA]	Voltage [V]	Avg. Power Generated [mW]	Avg. Power Consumed [mW]
2.7	234/25	21	3.4	3.2	11.95	0.394	0.197	1.193
2.1	327/35	21	4.9	4.5	17.55	0.656	0.455	
1	420/45	22	5.8	5.5	19.54	0.842	0.967	
0.5	514/55	22	6.6	9.5	21.55	0.958	1.450	
1.61	560/60	23	7.7	8.2	26.57	1.483	2.764	
0.2	420/45	22	7.4	6.7	26.98	1.557	3.906	
0.43	514/55	23	7.3	6.7	24.63	1.705	3.898	
2.1	327/35	21	5.2	4.9	20.75	2.076	2.319	
0.45	234/25	21	4.5	4.3	16.62	2.016	1.894	

4.2.2 Field Route Simulation – Unloaded Railcar

Table 4 displays the performance analysis of the thermoelectric energy harvester under an empty railcar load. The overall average power output throughout the test was 1.65 mW. The lowest recorded power generated occurred at the beginning of the test, producing 0.17 mW at a speed of 40.2 $\frac{km}{h}$ (25 mph), with measured temperature gradients of 3.5°C (6.3°F) on the leading side and 3.6°C (6.5°F) on the trailing side. Conversely, the highest instantaneous power output was observed during the final speed segment, also at 40.2 $\frac{km}{h}$ (25 mph), achieving 3.3 mW. The corresponding temperature differentials were 6°C (10.8°F) on the leading face and 5.3°C (9.5°F) on the trailing face.

Similar to the loaded condition, the supercapacitors were able to charge 2 V from the overall route, which made the system operate solely on the thermoelectric energy harvester.

Table 4: Results of thermoelectric energy harvester performance for the simulated field route at 17% railcar load – Defective bearing

Time [h]	**Speed [rpm]/ [mph]**	**Avg. T_{amb} [°C]**	**ΔT Leading [°C]**	**ΔT Trailing [°C]**	**Avg. Current Produced [mA]**	**Voltage [V]**	**Avg. Power Generated [mW]**	**Avg. Power Consumed [mW]**
2.7	234/25	21	3.5	3.6	12.04	0.370	0.175	1.193
2.1	327/35	22	3.1	2.8	16.48	0.613	0.395	
1	420/45	21	4.7	4.4	19.32	0.776	0.786	
0.5	514/55	21	5.7	5.1	19.92	0.874	1.123	
1.61	560/60	21	5.8	5.3	21.58	1.231	1.621	
0.2	420/45	23	6.6	5.8	22.51	1.281	2.181	
0.43	514/55	23	6.3	5.7	23.85	1.408	2.758	
2.1	327/35	22	6.2	5.4	19.75	1.876	2.541	
0.45	234/25	21	6	5.3	16.01	1.987	3.309	

CHAPTER V

CONCLUSIONS AND FUTURE WORK

The maintenance of railways has increased the demand for autonomous and unmanned monitoring to ensure safety and efficient transport of freight. Advancement in sensor technologies has allowed the introduction and implementation of onboard health monitoring devices that are capable of continuously assessing the health of important train components. Real-time data can be used by rail operators to schedule preventive maintenance. However, due to the nature of continuous monitoring the sensor modules require a sufficient energy source to collect and transmit data. Several energy harvesting methods have been considered by previous researchers, and for this study, the thermoelectric energy harvesting was selected due to its feasibility and practical application. The UTCRS team validated a thermoelectric energy harvester prototype with a wireless onboard condition monitoring device on a bearing test rig. However, the main challenge was to further enhance power generation with lower temperature gradients since some components of the electrical assembly were not able to meet self-start power requirements.

5.1 Non-Homogenous Temperature Effect On Thermoelectric Generators

During operation it is almost inevitable for the thermoelectric generators to undergo different temperature gradients between units that are connected electrically in a series array. To determine the impact of this effect an experimental study was performed on different electrical configurations for a system with two TEGs in series.

First, a single TEG array was used to determine control values and to later compare the performance of the other configurations. A relationship was devised to correlate the percentage of temperature gradient between the weaker TEG to the stronger TEG. More specifically, the temperature differential across the weaker TEG needs to be at least 41.1% of the temperature gradient of the stronger TEG to have a positive value on the net available power.

As seen during testing, the optimal solution would be a system with isolated TEGs with their own boost converters, however each single unit will need to be able to surpass the threshold voltage for their respective boost converter. The main reason for employing two TEGs is to enable energy harvesting independent of the train's direction of travel as airflow may vary.

5.2 Laboratory Testing Results

To assess the performance of the optimized UTCRS thermoelectric energy harvester, experimental results were analyzed and compared to the general power consumption of an onboard bearing health monitoring system. The preliminary standard tests indicated that the temperature gradients needed for the boost converter to operate were as low as 6°C, with both loading conditions.

As previously described the primary limitation of the UTCRS thermoelectric energy harvester was the need for a low-power boost converter. This was addressed through the replacement of the generic boost converter to the E-Peas AEM20940. Unlike the previous circuitry, the E-Peas AEM20940 is able to obtain the MPP during operation withstanding the power fluctuations from energy harvesting.

A route was simulated utilizing the UCTRS bearing test rig in order to evaluate the performance of the thermoelectric energy harvester while supplying power to an onboard condition monitoring device. To clarify, the board's consumption power was a version of

firmware that sets features of collecting, analyzing, and transmitting data. However, this firmware version was optimized to reduce power consumption, based on the results of the performed experiments. During these tests, the condition monitoring device was able to operate solely on the thermoelectric energy harvester towards the end of the route, replacing the primary batteries. This outcome indicates that although the energy harvester was able to produce power for low temperature gradients, it was ultimately insufficient for the device's power demands without supplementary source of energy.

5.3 Challenges

The validation of this energy harvester confirms a good outcome for the future of thermoelectric energy harvesting for the condition monitoring of rolling stock. However, there is still need for improvement in areas like design and charging circuitry.

One of the objectives for this energy harvester was to be a universal fit for different bearing class adapters. However, the dimensions of the thermoelectric generator (40×40 mm) used for this prototype do not fulfill this requirement. Field testing revealed that the module exceeded the available space on the leading and trailing sides of the adapter, discarding this test due to installation constraints. Although a smaller thermoelectric generator (30×30 mm) was evaluated in the previous prototype, it was not capable of operating effectively under low temperature gradients, such as those observed during route simulations.

Another challenge identified was the thermal imbalance between TEG units likely to occur during field service operations. The electrical configuration could be improved by the implementation of switching mechanisms in the system. Specifically, if the temperature differential of the weaker TEG contributes less than 41.1% of the temperature differential on the stronger TEG it should be isolated to prevent a negative impact on the overall power output.

5.4 Future Work

Should the thermoelectric energy harvester be selected for further optimization, the existing design limitations could be addressed. A key advantage of the thermoelectric generator is their design flexibility, which enables customization to meet specific application requirements and to overcome installation constraints. This adaptability makes them well-suited to be integrated into onboard monitoring systems for rolling stock. Additionally, there exists opportunities to advance research into the thermoelectric materials utilized for energy generation to increase their efficiency.

The critical role of onboard monitoring systems in assessing the health of freight components demands a reliable and efficient energy harvesting solution. To ensure consistent power availability for continuous monitoring, it is recommended to explore different energy harvesting systems. In particular, photovoltaic systems offer a promising alternative with their technological maturity and potential compatibility with the power demands of onboard condition monitoring devices. Further comparative studies of thermoelectric and photovoltaic systems could help determine the most effective strategy for long-term deployment in real-world operational conditions.

REFERENCES

[1] Federal Railroad Administration. (n.d.). Train accidents by fiscal and calendar year with rates. U.S. Department of Transportation. Retrieved from https://safetydata.fra.dot.gov/officeofsafety/publicsite/query/TrainAccidentsFYCYWithRates.aspx

[2] Federal Railroad Administration. (n.d.). Rail climate considerations. U.S. Department of Transportation. Retrieved from https://railroads.dot.gov/rail-network-development/environment/rail-climate-considerations

[3] Tarawneh, C., Aranda, J., Hernandez, V., Crown, S., & Montalvo, J. (2019). An investigation into wayside hot-box detector efficacy and optimization. International Journal of Rail Transportation, 8(3), 264–284. https://doi.org/10.1080/23248378.2019.1636721

[4] Apna Technologies & Solutions. (n.d.). [Image of wayside hot box detector] [Photograph]. ApnaTech. https://apnatech.com/?page_id=240

[5] National Transportation Safety Board. (2024). Norfolk Southern Railway derailment and hazardous materials release (NTSB/RAR-24/01). https://www.ntsb.gov/investigations/Pages/RRD23MR005.aspx

[6] Puskar, G. (2023, March 7). How the Ohio train derailment unfolded. [Photograph]. The New York Times. https://www.nytimes.com/article/ohio-train-derailment-timeline.html

[7] Southern, C., Rennison, D., & Kopke, U. (2004). RailBAM - an Advanced Bearing Acoustic Monitor: Initial Operational Performance Results. In CORE 2004: New Horizons for Rail. Railway Technical Society of Australasia. https://search.informit.org/doi/10.3316/informit.424528912570715

[8] Federal Railroad Administration. (2019). An implementation guide for wayside detector systems (Report No. DOT/FRA/ORD-19/20). U.S. Department of Transportation. https://www.fra.dot.gov/eLib/details/L20120

[9] Apna Technologies & Solutions. (n.d.). [Image of Track side Microphone Array] [Photograph]. ApnaTech. https://apnatech.com/?page_id=285

[10] Wabtec Corporation. (n.d.). Image of the RailBAM acoustic bearing monitoring system [Photograph]. Wabtec Corporation. https://www.wabteccorp.com/asset-management-Track-RailBAM-brochure

[11] Newman, R. R., Leedham, R. C., Tabacchi, J., Purta, D., Maderer, G. G., & Galli, R. (1990, April). Hot bearing detection with the SMART-BOLT. In IEEE Technical Papers Presented at the Joint ASME/IEEE/AAR Railroad Conference (Association of American Railroads) (pp. 105-110).

[12] Donelson, J., Edwards, M. C., Filkins, M. H., Punwani, S. K., Stewart, M. F., Toth, D. G., & Zavis, W. M. (2005, March). Performance of an on-board monitoring system in a revenue

service demonstration. In Proceedings of the 2005 ASME/IEEE Joint Rail Conference, 2005. (pp. 123-129). IEEE.

[13] Campbell, T., & Sharif, H. (2021). Onboard Monitoring and Control–Wireless Sensor Networks Systems Integration (No. DOT/FRA/ORD-21/21). United States. Department of Transportation. Federal Railroad Administration. Office of Research, Development, and Technology.

[14] HUM Industrial Technology. (2024, May 15). Another day, another install – our Boomerang™ bearing monitoring system is live on this unit! [Image attached] [Post]. LinkedIn. https://www.linkedin.com/posts/hum-industrial-technology-llc_another-day-another-install-our-boomerang-activity-7175966660355399680-sJDp

[15] Priya, S., & Inman, D. J. (Eds.). (2009). Energy harvesting technologies (Vol. 21, p. 2). New York: Springer.

[16] Kazmierski, T. J., & Beeby, S. (2011). Energy harvesting systems. Principles, Modeling and Applications.

[17] Hao, D., Zhang, T., Guo, L., Feng, Y., Zhang, Z., & Yuan, Y. (2021). A High-Efficiency, Portable Solar Energy-Harvesting System Based on a Foldable-Wings Mechanism for Self-Powered Applications in Railways. Energy Technology, 9(4), 2000794.

[18] Morita, Y., Honda, M., Kuraoka, T., Fukasawa, Y., Mitoma, Y., Yoshizumi, H., & Hayashiya, H. (2012, November). Analysis of local smoothing effect on the PV on Tokyo station. In 2012 International Conference on Renewable Energy Research and Applications (ICRERA) (pp. 1-6). IEEE.

[19] Cii, S., Tomasini, G., Bacci, M. L., & Tarsitano, D. (2020). Solar wireless sensor nodes for condition monitoring of freight trains. IEEE Transactions on Intelligent Transportation Systems, 23(5), 3995-4007.

[20] Vasisht, M. S., Vashista, G. A., Srinivasan, J., & Ramasesha, S. K. (2017). Rail coaches with rooftop solar photovoltaic systems: A feasibility study. Energy, 118, 684-691.

[21] Dziadak, B., Kucharek, M., & Starzyński, J. (2022). Powering the WSN node for monitoring rail car parameters, using a piezoelectric energy harvester. Energies, 15(5), 1641.

[22] Shan, G., Wang, D., Chew, Z. J., & Zhu, M. (2023). A high-power, robust piezoelectric energy harvester for wireless sensor networks in railway applications. Sensors and Actuators A: Physical, 360, 114525.

[23] Hadas, Z., Rubes, O., Ksica, F., & Chalupa, J. (2022). Kinetic electromagnetic energy harvester for railway applications—development and test with wireless sensor. Sensors, 22(3), 905.

[24] Lin, T., Wang, J. J., & Zuo, L. (2018). Efficient electromagnetic energy harvester for railroad transportation. Mechatronics, 53, 277-286.

[25] De Pasquale, G., Somà, A., & Zampieri, N. (2012). Design, simulation, and testing of energy harvesters with magnetic suspensions for the generation of electricity from freight train vibrations.

[26] Shen, Z. G., Tian, L. L., & Liu, X. (2019). Automotive exhaust thermoelectric generators: Current status, challenges and future prospects. Energy Conversion and Management, 195, 1138-1173.

[27] Kim, T. Y., Kwak, J., & Kim, B. W. (2018). Energy harvesting performance of hexagonal shaped thermoelectric generator for passenger vehicle applications: An experimental approach. Energy Conversion and Management, 160, 14-21.

[28] Ahn, D., & Choi, K. (2018). Performance evaluation of thermoelectric energy harvesting system on operating rolling stock. Micromachines, 9(7), 359.

[29] Amaro, M., Jr. (2021). Developing a prototype energy harvesting device for powering wireless onboard condition monitoring sensor modules for railway service (Master's thesis). The University of Texas Rio Grande Valley.

[30] Montecucco, A., Siviter, J., & Knox, A. R. (2014). The effect of temperature mismatch on thermoelectric generators electrically connected in series and parallel. Applied Energy, 123, 47-54.

[31] Capitanachi, D., de Leon, G., Rodriguez, C., Tarawneh, C., & Foltz, H. (2024, May). Powering Onboard Bearing Health Monitoring Sensors With Thermoelectric Generators Under Non-Uniform Temperatures. In ASME/IEEE Joint Rail Conference (Vol. 87776, p. V001T05A006). American Society of Mechanical Engineers.

[32] Calc Maps [Internet] [Accessed 2025 March 19] Available from: https://www.calcmaps.com/map-distance

VITA

Danna Cecilia Capitanachi Avila was born in Reynosa, Tamps., Mexico. She obtained her Bachelor of Science in Mechanical Engineering at the University of Texas Rio Grande Valley (UTRGV) and graduated Cum Laude in 2022. Her research in the University Transportation Center for Railway Safety (UTCRS) focuses on energy harvesting for the upkeep of onboard sensors for railroad service. Research has provided opportunities such as being able to take part in conferences, journals, and the Dwight D. Eisenhower Transportation Fellowship Program in 2023 and 2024 to present her projects. She is currently pursuing her Master of Science in Mechanical Engineering and is scheduled to graduate in July 2025.

Danna can be contacted by email at danna.capitanachi@outlook.com.